2016

Polarization Dependent Switching of Asymmetric Nanorings with a Circular Field

Nihar R. Pradhan
Mount Holyoke College

Mark T. Tuominen
University of Massachusetts Amherst

Katherine E. Aidala
Mount Holyoke College

Recommended Citation
Pradhan, Nihar R.; Tuominen, Mark T.; and Aidala, Katherine E., "Polarization Dependent Switching of Asymmetric Nanorings with a Circular Field" (2016). *AIP Advances*. 1244.
http://dx.doi.org/10.1063/1.4939698

Polarization dependent switching of asymmetric nanorings with a circular field

Nihar R. Pradhan, Mark T. Tuominen, and Katherine E. Aidala

Citation: AIP Advances **6**, 015302 (2016); doi: 10.1063/1.4939698
View online: http://dx.doi.org/10.1063/1.4939698
View Table of Contents: http://aip.scitation.org/toc/adv/6/1
Published by the American Institute of Physics

Polarization dependent switching of asymmetric nanorings with a circular field

Nihar R. Pradhan,[1,2] Mark T. Tuominen,[2] and Katherine E. Aidala[1]
[1]*Department of Physics, Mount Holyoke College, South Hadley, MA 01075, USA*
[2]*Department of Physics, University of Massachusetts, Amherst, MA 01003, USA*

(Received 6 September 2015; accepted 28 December 2015; published online 5 January 2016)

We experimentally investigated the switching from onion to vortex states in asymmetric cobalt nanorings by an applied circular field. An in-plane field is applied along the symmetric or asymmetric axis of the ring to establish domain walls (DWs) with symmetric or asymmetric polarization. A circular field is then applied to switch from the onion state to the vortex state, moving the DWs in the process. The asymmetry of the ring leads to different switching fields depending on the location of the DWs and direction of applied field. For polarization along the asymmetric axis, the field required to move the DWs to the narrow side of the ring is smaller than the field required to move the DWs to the larger side of the ring. For polarization along the symmetric axis, establishing one DW in the narrow side and one on the wide side, the field required to switch to the vortex state is an intermediate value. [http://dx.doi.org/10.1063/1.4939698]

Ferromagnetic nanorings have generated interest due to their unique states, including the flux-closed vortex state in which the moments align circumferentially, generating no stray magnetic field in a symmetric ring. The vortex state can have either clockwise (CW) or counterclockwise (CCW) circulation, which have degenerate energies in uniform applied fields. Nanorings have been proposed as data storage elements,[1–9] taking advantage of the stable equilibrium CW and CCW configurations with no stray field. Understanding and controlling the switching of nanorings is of fundamental interest and critical to progress towards data storage applications. Prior work generally uses uniform in-plane fields to explore the switching behavior of these rings.[10] External uniform magnetic fields cannot select between the CW and CCW state. Introducing asymmetry into the ring allows for control over the vortex circulation with a uniform in-plane field, using the asymmetry to determine the motion of DWs and consequently the final circulation of the vortex, whether through fabricating an asymmetric ring (AR)[11–14] or introducing magnetic structures outside the ring to break the symmetry.[15,16] Spin polarized current also enables control over the vortex circulation.[4,17,18] We recently reported the motion of 180° DWs and control of vortex circulation in symmetric and asymmetric permalloy and cobalt nanorings facilitated by a local circular field made by passing current through the center of a ring using an atomic force microscope (AFM) tip.[19,20] Previously, we demonstrated the switching from onion to vortex state in symmetric and asymmetric rings by applying a circular field at the center, as well as vortex to vortex switching in asymmetric rings. Here we investigate the onion to vortex switching in asymmetric nanorings, specifically initializing the onion state along the symmetric or asymmetric axes.

To initialize the ring, we first apply a uniform in-plane field to polarize the nanorings along the desired axis (Fig. 1). Because the hole of the ring is off-center, the width of the ring arm varies along the circumference. The width of the arm determines the width of the DW and consequently the energy of the DW. It is energetically favorable for a DW to move to a narrower location along the ring. If the ring is polarized along the asymmetric axis, creating DWs in a location of intermediate width (see Fig. 1(b)), the DWs will move to the narrow side and annihilate as the uniform field is reduced. The DWs will only remain in the position sketched if there is some pinning potential that prevents

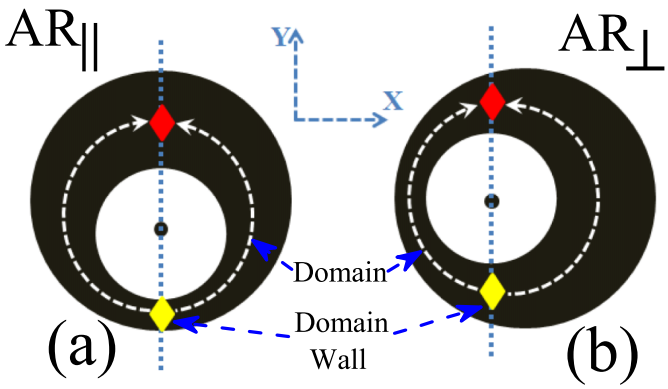

FIG. 1. Schematic of the two polarizations of the onion state in an asymmetric nanoring, with the 180° DWs indicated by red and yellow diamonds. (a) The in-plane initialization field was applied parallel to the symmetric axis of the ring, forming DWs in the narrow and wide ends, and labelled $AR_{\|}$. (b) The initial field was applied perpendicular to the symmetric axis of the ring, forming two identical DWs, and labelled $AR_{\perp}$.

the walls from moving towards the narrower side. If the ring is polarized along the symmetric axis, with one wall in the narrowest part and one in the widest, the wide wall will move to the narrow end, and its direction of motion (and the resulting vortex circulation) cannot be controlled with a uniform applied field. With the ability to apply a circular field, we can fully control the motion of the DWs and the resulting vortex circulation, allowing us to fully probe the switching processes.

Arrays of asymmetric nanorings with an outer diameter of 900 nm and inner diameter of 540 nm were fabricated on a gold-coated Si wafer using electron-beam lithography. The inner diameter was off center by 120 nm to introduce the geometric asymmetry. A 15 nm Co film was deposited by electron beam evaporation. A platinum layer of 4 nm was deposited on the top of Co to reduce the oxidation. The detailed fabrication procedure can be found elsewhere.[19,20] An Asylum Research MFP-3D atomic force microscope was used to manipulate the magnetic states of each individual nanoring. Initially, an in-plane magnetic field of ± 2500 Oe was temporarily applied to the sample with the variable field module of the microscope. The magnetic states of the nanorings at remanence were imaged with a high coercivity magnetic force microscope (MFM) tip at a scan height of 50 nm. The MFM tip was replaced by a solid platinum (Pt) metal tip purchased from Rocky Mountain Nanotechnology,[21] brought into contact with the conducting surface at the center of the selected individual ring, and the desired amount of current was passed through the tip. The current passed through the center of the ring was measured by recording the voltage drop across a known resistor connected in series with the tip. The detailed circuit diagram can be found elsewhere.[19,20] The strength of the applied circular field was calculated by Ampere's law, assuming an infinitely long wire and using the average radius of the asymmetric nanoring. The experimental procedure consisted of first imaging the magnetic state in zero field with an MFM tip, switching to the solid Pt tip and passing current, and then returning to the MFM tip and locating the same ring to image the resulting magnetic state. If the applied circular field was insufficient to change the magnetic state, then the above procedure was repeated, increasing the field strength until the switching of magnetic states occurred. All measurements were performed at room temperature, in air.

We studied the switching of asymmetric nanorings from the onion to vortex state, examining the dependence of switching field on the initial polarization of the ring along the symmetric and asymmetric axis. Figure 1 presents the schematic of the two different polarizations of the onion states. In Fig. 1(a), the initial in-plane field was applied along the Y-axis, which is parallel to the symmetric axis of the ring, and we label this state $AR_{\|}$. The head-to-head (H-H) DW appears on the widest section of the ring, and the tail-to-tail (T-T) DW appears on the narrowest ring arm, forming two domains equal in sizes and opposite in their direction of circulation. In Fig. 1(b), the initial field was applied perpendicular to the symmetric axis, and this state is labelled $AR_{\perp}$. The two DWs have the same length and are found between the narrowest and widest arm width.

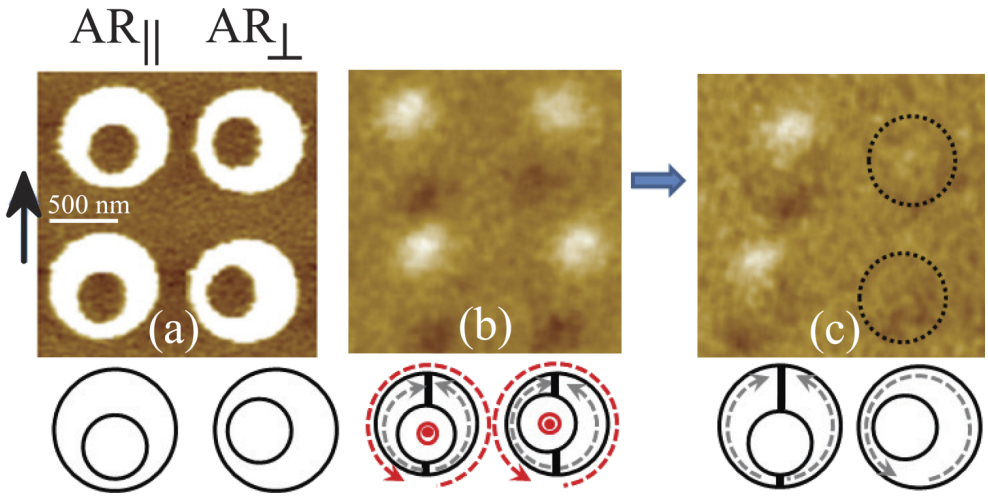

FIG. 2. (a) AFM height image of four asymmetric cobalt nanorings. The black arrow indicates the direction of the initialization field. (b) MFM image at remanence after removing the in-plane applied field. Bottom sketch indicates the magnetic states of the rings, and the red-dashed arrow indicates the location and direction of the applied circular field. (c) MFM image of rings after applying the circular field, with schematic diagrams of the magnetization below.

Figure 2(a) shows the AFM height image of four identical asymmetric nanorings, with two different orientations. The sketch below the image shows the orientation of the rings, and the initial polarizing field is applied along Y-direction (indicated by the black arrow). The left two rings are in the $AR_{\parallel}$ state, and the right two rings are $AR_{\perp}$. The MFM image reveals all four rings are in the onion state at remanence, with the two 180° DWs indicated by bright and dark contrasts in Fig. 2(b). The schematic drawn below the MFM image shows the magnetic configurations of the $AR_{\parallel}$ and $AR_{\perp}$ states. The dashed-red circular arrow represents the direction of the applied circular field, created by passing current through the center of the ring. We applied a CCW circular field of 171 Oe on all four rings, resulting from 35 mA of current passed through the center of the rings. This current corresponds to a current density on the order of 10^9 $A\ cm^{-2}$, assuming a 25 nm tip radius, and is ramped up to 35 mA and back down over 1 second. Figure 2(c) shows the MFM image of the resulting magnetic states of all four rings after applying the circular field. The $AR_{\parallel}$ rings remained in the same onion state while the $AR_{\perp}$ rings showed very weak MFM contrast, indicating the rings switched to the CCW-vortex state. The sketches below the MFM image shows the resulting magnetic configurations of the nanorings after applying the circular field. The applied CCW circular field on the $AR_{\perp}$ rings grew the wider domain by moving the two 180° DWs towards the narrowest section of the ring, where the DWs annihilate to form the vortex state. The energy of the DW is proportional to the width and thickness of the ring arm,[11,15] and this motion of DWs to the narrow side of the ring would be downhill in energy in a perfect ring. In $AR_{\parallel}$, one of the two 180° DWs is trapped at the narrowest width of the ring, which reduces the total energy and is more stable than both DWs in $AR_{\perp}$. The strength of the applied field was insufficient to form the vortex state. The applied field did not move the DW on the widest section of the ring. We measured the average switching field from the $AR_{\perp}$ state to the CCW vortex state to be 71±5 Oe, where the uncertainty is the standard deviation across ten nanorings.

Figure 3 shows the switching of the $AR_{\perp}$ nanoring from the onion to CW-vortex state, moving the DWs to the wide end of the ring. The AFM height image of two $AR_{\perp}$ nanorings is shown in Fig. 3(a), with the direction of the initial in-plane applied field indicated by the arrow between the two rings. The MFM image at remanence shown in Fig. 3(b) reveals the rings are in the onion state, indicated by the sketches below the MFM images. Clockwise circular field was applied to the left ring by passing 46 mA of current (254 Oe) through the center of the left ring, indicated by the red dashed arrow around the sketch. To determine the switching field, the applied current was increased stepwise from the lower value determined by the switching in Fig. 2, and we show the magnetic state after switching in Fig. 3(c). The ring on the left side showed very weak MFM contrast, which

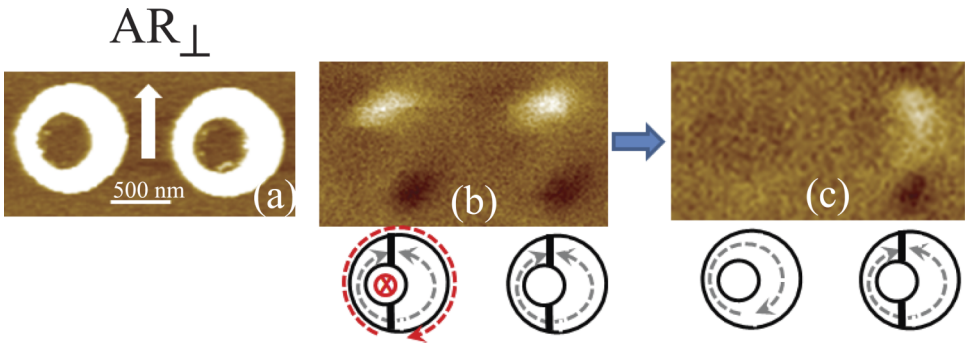

FIG. 3. (a) AFM height image of two asymmetric cobalt nanorings. Arrow indicates the direction of the initial in-plane field, perpendicular to the symmetric axis. (b) MFM image of rings at remanence after removing the in-plane applied field. The red-dashed arrow around the cartoon below the MFM image indicates the location and direction of the applied circular field. (c) MFM image of rings after applying the circular field, with schematic diagrams of the magnetization below.

confirmed that the ring switched to the CW-vortex state. The ring on the right side was unperturbed by the field applied on the left ring and remained in the onion state. Compared to the switching field for $AR_{\perp}$ when the DWs move to the narrow side of the ring ($171 \pm 5\ Oe$), the switching field required to move the DWs to the wider end is significantly larger ($254 \pm 15\ Oe$).

For the $AR_{\parallel}$ state, one DW is initialized at the narrow end and one on the wide end. This configuration is more stable than $AR_{\perp}$ when moving the DWs to the narrow side, as shown in Fig. 2. We performed the same experiment, increasing the field strength until we observed switching into the vortex state. Figure 4(a) shows the AFM height image of two $AR_{\parallel}$ nanorings, with the corresponding MFM images at remanence in Fig. 4(b), confirming the rings are in onion states. The cartoons below the MFM image show the configuration of magnetic states. A CCW circular field was applied on the right ring by passing a 40 mA current (195 Oe) through the center of the ring. The red arrow indicates the direction of applied circular field on the ring. The resulting magnetic state is shown in Fig. 4(c). The weak magnetic contrast on the right ring indicates the magnetic state switched from onion to the CCW-vortex state, while the magnetic state of the left ring remain unchanged. The measured switching field is an intermediate value og 195±9 Oe, between the two different directions of the $AR_{\perp}$ states.

To better understand the switching process, we performed micromagnetic simulations using OOMMF[22] on an ideal asymmetric Co nanoring with the same geometry. We used standard parameters for Cobalt, but with zero crystalline anisotropy given the polycrystalline deposition of our material, a cell size of 4nm in x and y, a damping parameter of 0.5, and the magnetization state evolves until the $\frac{d\mathbf{M}}{dt} < 0.1$ deg/ns. The initial magnetization states are shown in Fig. 5(a) and 5(d)

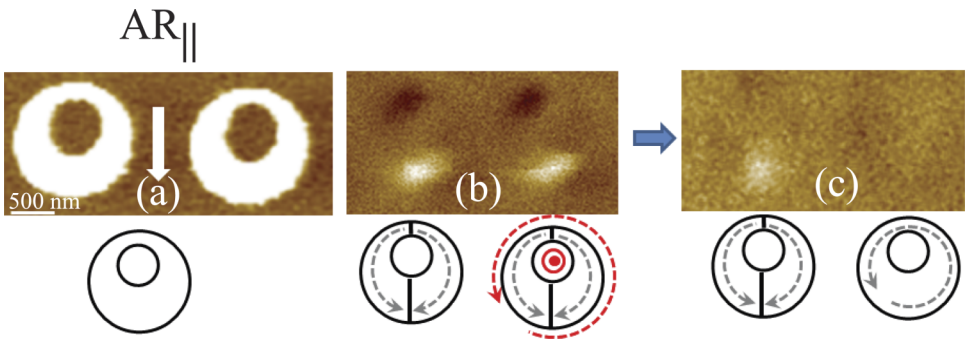

FIG. 4. (a) AFM height image of two asymmetric cobalt nanorings. Arrow indicates the direction of the initial in-plane field, parallel to the symmetric axis. (b) MFM image of rings at remanence after removing the in-plane applied field. The red-dashed arrow around the cartoon below the MFM image indicates the location and direction of the applied circular field. (c) MFM image of rings after applying the circular field, with schematic diagrams of the magnetization below.

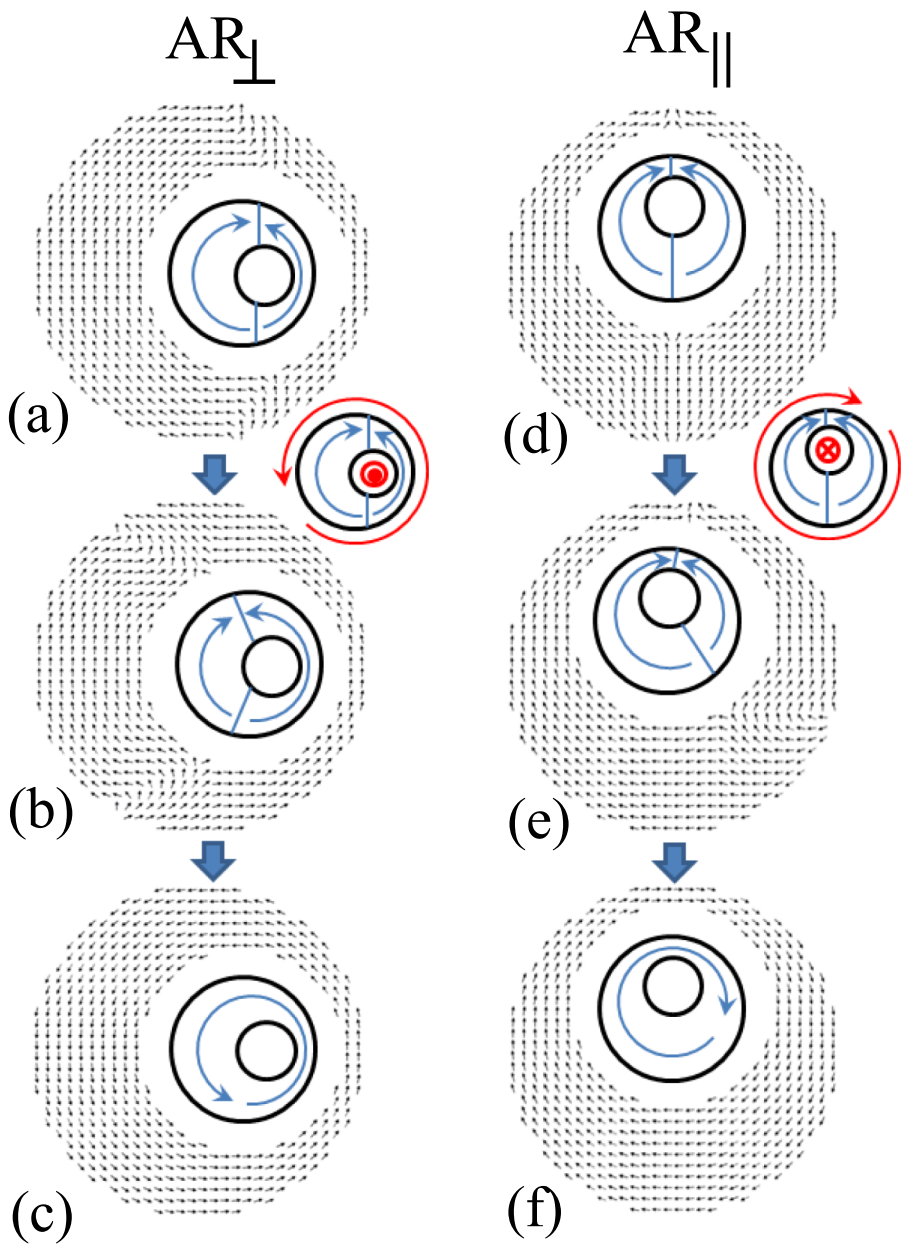

FIG. 5. (a) Simulated magnetization states of $AR_{\perp}$ and $AR_{\parallel}$ nanorings shown in Fig. 3 and Fig. 4. (a) and (d) are the initial magnetization states after the rings are polarized perpendicular and parallel to the symmetric axis, respectively. The direction of the applied circular field is shown by the red arrows around the schematics. (b) and (e) are intermediate states that show the direction of the DW motion. (c) and (f) are the final magnetization states after the field is applied.

after polarizing along the asymmetric and symmetric axis respectively. The schematics within the simulated images indicate the magnetization state of the rings. We increased the applied CCW circular field on the $AR_{\perp}$ ring (Fig. 5(a)), indicated by the red arrow. The ring switched at 164 Oe, which corresponds to a 25 mA current through the center. We show the motion of the DWs in Fig. 5(b), which is a snapshot of an intermediate state, revealing both DWs move towards the wide end before they annihilate. This symmetric motion is presumably due to identical pinning potentials of the two walls, such that they both begin to move for the same field strength. The final magnetization state of the CCW vortex is shown in Fig. 5(c). Similarly, we increased the applied CW circular field to 66 Oe, corresponding to 10 mA current through the center of $AR_{\parallel}$ ring. The motion of the DWs is shown in Fig. 5(e), revealing the DW on the wide end of the ring moves to the narrow end,

while the other DW is stationary. This motion is expected because the energy of the DW on the wide side of the ring will decrease as it moves to the narrower side, while the wall at the narrow side feels a stronger pinning potential. The final CW magnetization is shown in Fig. 5(f), after the DWs annihilate in the narrow end. The simulations confirm that a larger switching field is required when the ring is initialized along the asymmetric axis ($AR_{\perp}$) and the DWs are moved to the wider end than when the ring is initialized along the symmetric axis ($AR_{\parallel}$), and the wide DW moves to the narrow end. We do not expect the switching fields to quantitatively agree with our experiments, because the simulation is at 0 K (increasing switching fields) and without fabrication defects (decreasing switching fields). Our experimental rings contain pinning sites due to inhomogeneities, creating a local potential well that must be overcome by the applied circular field.

In conclusion, we investigated the onion to vortex switching process in asymmetric cobalt nanorings, dependent upon their initial polarization relative to the axis of symmetry. The polarization field was applied along either the symmetric or asymmetric axis. The circular magnetic field was applied by passing current through the center of the ring using a solid metal AFM tip. The experimental results conclude that the switching field depends upon the direction of initial polarization that determines initial position of DWs on the ring arm. We observed the smallest switching field in $AR_{\perp}$ from onion to CCW-vortex state (where the DWs move towards the narrowest arm of the ring) and the highest switching field in onion to CW-vortex state (where DWs move towards the widest arm of the ring). The observed switching field from onion to CCW-vortex state of $AR_{\parallel}$ was intermediate of the above two switching fields. The switching field will also depend upon other parameters such as the thickness, diameter and asymmetry of the nanorings. Simulations confirm this relationship, though pinning of the DWs in any real structure affects the switching field.

The authors acknowledged the support by NSF grants No. DMR 0906832, 097201, 1208042, 1207924, and the NSF Center for Hierarchical Manufacturing at the University of Massachusetts, Amherst (CMMI-0531171). Simulations were performed with the computing facilities provided by the Center for Nanoscale Systems (CNS) at Harvard University (NSF award ECS-0335765), a member of the National Nanotechnology Infrastructure Network (NNIN).

[1] J. G. Zhu, Y. F. Zheng, and G. A. Prinz, J. Appl. Phys. **87**, 6668 (2000).
[2] Gabriel D. Chaves-O'Flynn, A. D. Kent, and D. L. Stein, Phys. Rev. B **79**, 184421 (2009).
[3] C. B. Muratov and V. V. Osipov, IEEE Trans. Magn. **45**, 3207 (2009).
[4] H. Xu, X. Chen, J. Hua, and J. Liu, J. Magn. Magn. Mater. **321**, 3698 (2009).
[5] M. T. Moneck and J.-G. Zhu, J. Appl. Phys. **99**, 08H709 (2006).
[6] T. J. Hayward, J. Llandro, R. B. Balsod, J. A. C. Bland, F. J. Castano, D. Morecroft, and C. A. Ross, Appl. Phys. Lett. **89**, 112510 (2006).
[7] K. Martens, D. L. Stein, and A. D. Kent, Phys. Rev. B **73**, 054413 (2006).
[8] X. Zhu and J.-G. Zhu, IEEE Trans. Magn. **39**, 2854 (2003).
[9] C. A. Ross and F. J. Castano, "Magnetic memory elements using 360-degree walls," US Patent 6,906,369 B2 (2005).
[10] C. A. F. Vaz, T. J. Hayward, J. Llandro, F. Schackert, D. Morecroft, J. A. C. Bland, M. Klaui, M. Laufenberg, D. Backes, U. Rudiger, F. J. Castao, C. A. Ross, L. J. Heyderman, F. Nolting, A. Locatelli, G. Faini, S. Cherifi, and W. Wernsdorfer, **19**, 255207 (2007).
[11] F. Q. Zhu, G. W. Chern, O. Tchernyshyov, X. C. Zhu, and C. L. Chien, Phys. Rev. Lett. **96**, 027205 (2006).
[12] F. Giesen, J. Podbielski, B. Botters, and D. Grundler, Phys. Rev. B **75**, 184425 (2007).
[13] E. Saitoh, M. Kawabata, K. Harii, H. Miyajima, and T. Yamaoka, J. Appl. Phys. **95**, 1986 (2004).
[14] P. Vavassori, R. Bovolenta, V. Metlushko, and B. Llic, J. Appl. Phys. **99**, 053902 (2006).
[15] E. Sirotkin and F. Y. Ogrin, IEEE Trans. Magn. **46**(6), 1840 (2010).
[16] Chunghee Nam, B.G. Ng, F. J. Castano, M. D. Mascaro, and C. A. Ross, Appl. Phys. Lett. **94**, 082501 (2009).
[17] T. Yang, M. Hara, A. Hirohata, T. Kimura, and Y. Otani, Appl. Phys. Lett. **90**, 022504 (2007).
[18] H. X. Wei, M. C. Hickey, G. I. R. Anderson, X. F. Han, and C. H. Marrows, Phys, Rev, B **77**, 132401 (2008).
[19] T. Yang, N. R. Pradhan, A. Goldman, A. Licht, Y. Li, M. Kemei, M. T. Tuominen, and K. E. Aidala, Appl. Phys. Lett. **87**, 6668 (2011).
[20] N. R. Pradhan, A. Licht, Y. Li, Y. Sun, M. T. Tuominen, and K. E. Aidala, Nanotechnology **22**, 485705 (2011).
[21] Rocky Mountain Nanotechnology, LLC. (http://rmnano.com/).
[22] The Object Oriented MicroMagnetic Framework developed by NIST (http://math.nist.gov/oommf/).